Simple Quasi-Exact Filtered Backprojection Algorithms for Long-Object Problem in Helical Cone-Beam Tomography

Hiroyuki Kudo[1], Frédéric Noo[2], and Michel Defrise[3]
[1]Institute of Information Sciences and Electronics, University of Tsukuba, Tsukuba 305-8573, Japan
[2]Institute of Electricity Montefiore, University of Liege, Belgium
[3]Department of Nuclear Medicine, Free University of Brussels, Belgium

I. Introduction

Since the development of multi-slice helical CT, cone-beam reconstruction with a helical vertex path is receiving increasing attention. The current multi-slice CT scanners are adopting a class of approximate reconstruction algorithms which can be viewed an extension of the 2-D FBP algorithm. However, these approximate algorithms break down as the pitch of helix becomes large. In fact, major companies are beginning to develop a large area detector having more than 100 detector rows which allows a helical scan with a quite large pitch. This limitation of approximate algorithms motivated researchers to develop a class of exact reconstruction algorithms [1]-[6].

The reconstruction problems in helical cone-beam CT can be divided into the short-object (SO) problem and the long-object (LO) problem. The SO problem aims at reconstructing an object having a finite axial support when the helix is long enough to cover the object support. The LO problem aims at reconstructing a central region of interest (ROI) of a long object when the helix is long enough to cover the ROI but too short to cover the whole object. In 1998, Tam [1] and Kudo *et al.* [2] developed quasi-exact algorithms for the SO problem. In 2000, Schaller *et al.* [3], Defrise *et al.* [4], and Kudo *et al.* [5] extended the solutions to the SO problem to the LO problem. The resulting algorithms are called the Local-ROI (L-ROI) method [3],[6], the Zero-Boundary (ZB) method [4], and the Virtual-Circle (VC) method [5] in the literature. However, it is fair to say that these algorithms need rather complicated modifications to the quasi-exact algorithms for the SO problem.

The purpose of this paper is to develop new quasi-exact FBP algorithms to the LO problem. Similarly to the VC method [5], the algorithms can be viewed an extension of the quasi-exact FBP algorithm for the SO problem developed by Kudo *et al.* [2]. The main advantage of the proposed algorithms is their simplicity compared with the existing quasi-exact algorithms (L-ROI, ZB, and VC). The algorithms need only a few small changes to the quasi-exact FBP algorithm for the SO problem although their derivation involves rather different mathematical logic. We show simulation results which demonstrate that the proposed algorithms allow to reconstruct high-quality images indistinguishable from those by the VC method [5].

II. Proposed Algorithms

A. FBP Algorithm for Short-Object Problem

We first review the quasi-exact FBP algorithm for the SO problem derived by Kudo *et al.* [2] which is the basis of proposed algorithms for the LO problem. This review also helps to convince readers what modifications are necessary to convert the algorithm for the SO problem into the algorithms for the LO problem.

We use the same notations as in our previous papers [2],[5]. Let $f(\vec{r})$ denote an object supported inside a cylinder $\Omega = \{\vec{r} \mid x^2 + y^2 \leq Q^2\}$ where $\vec{r} = (x, y, z)^T$. We assume that cone-beam projections are measured along a finite segment of helix:

$$\vec{a}(\lambda) = (R\cos\lambda, R\sin\lambda, h\lambda)^T;\ \lambda_{\min} \leq \lambda \leq \lambda_{\max} \qquad (1)$$

where $2\pi h$ is the pitch and the range $[\lambda_{\min}, \lambda_{\max}]$ defines the length of helix. Let $g(u, v, \lambda)$ denote a cone-beam projection measured from the source point $\vec{a}(\lambda)$ where (u, v) denote the detector coordinates defined such that the u-axis coincides with the tangential direction of the helical path $\vec{a}'(\lambda)$. Let $D(\lambda)$ denote the detector plane corresponding to $\vec{a}(\lambda)$ where $D(\lambda)$ contains the z-axis. We assume that each cone-beam projection is measured over the finite region on the detector plane B which is bounded by the cone-beam projection of the upper turn of helix onto $D(\lambda)$ and by the cone-beam projection of the lower turn onto $D(\lambda)$. The explicit expression of B can be found in [1],[2]. This region B is known to be the minimum detector area compatible with exact reconstruction. Let $\chi_B(u, v)$ denote the indicator function of B. We also use a notation $g^\mu(s, t, \lambda)$ below to denote a cone-beam projection rotated by an angle μ on the detector plane where (s, t) denote the coordinates rotated by the angle μ. Kudo *et al.* [2] derived the FBP algorithm for the SO problem. This algorithm is quasi-exact when the axial support of the object is small compared with the length of helix such that $g(u, v, \lambda_{\min})$ and $g(u, v, \lambda_{\max})$ vanish over the region B. The algorithm is summarized as follows.

<Algorithm for SO Problem (Algorithm SO)>

[STEP 1] Weighting

$$g_1(u, v, \lambda) = \frac{R}{\sqrt{R^2 + u^2 + v^2}} g(u, v, \lambda) \qquad (2)$$

[STEP 2] Computation of Ramp Filtering Term

$$g^{Fr}(u,v,\lambda) = \frac{1}{2\pi}\int_{-\infty}^{\infty} du' h(u-u')\chi_B(u',v)g_1(u',v,\lambda) \tag{3}$$

where $h(\cdot)$ denotes the kernel of the ramp filter.

[STEP 3] Computation of Boundary Correction Term

$$S_\Delta^{(b)}(s,\mu,\lambda) = c_U(s,\mu)g_1^\mu(s,t_U,\lambda) + c_L(s,\mu)g_1^\mu(s,t_L,\lambda) \tag{4}$$

$$g^{Fb}(u,v,\lambda) = \frac{1}{4\pi^2}\frac{\partial}{\partial u}\int_{-\pi/2}^{\pi/2} d\mu S_\Delta^{(b)}(u\cos\mu + v\sin\mu,\mu,\lambda) \tag{5}$$

where t_U (or t_L) denotes the t-coordinate of the point on which the straight line $s = u\cos\mu + v\sin\mu$ intersects the upper (or lower) boundary of B. The explicit expressions of $c_U(s,\mu)$ and $c_L(s,\mu)$ can be found in Eq. (30) of [5].

[STEP 4] Backprojection

$$f(\vec{r}) = \int_{\lambda_{\min}}^{\lambda_{\max}} d\lambda \frac{R \parallel \vec{a}'(\lambda) \parallel}{[(\vec{r}-\vec{a}(\lambda))\cdot\vec{1}_w]^2}(g^{Fr}(u,v,\lambda)+g^{Fb}(u,v,\lambda)) \tag{6}$$

where $\vec{1}_w$ denotes the unit vector which is directed toward the detector center from $\vec{a}(\lambda)$.

The key feature of the above algorithm is that the filtered projection $g^{Fr} + g^{Fb}$ can be computed as a sum of the ramp filtering term applied to the truncated projection $\chi_B g_1$ and the boundary correction term which only depends on values of g_1 along the boundary of region B.

B. FBP Algorithms for Long-Object Problem

A blind use of the above FBP algorithm to the long object having a large axial support compared with the length of helix produces severe low-frequency artifacts [5]. This section describes two quasi-exact FBP algorithms which are derived from the mathematical logic outlined in Section II-C.

To describe the proposed algorithms, we need to define a region on the detector plane called the region $A(\lambda)$. Its definition is as follows. Let $P_{\min} = (u_{\min}(\lambda), v_{\min}(\lambda))$ (or $P_{\max} = (u_{\max}(\lambda), v_{\max}(\lambda))$) denote the cone-beam projection of the end point of helix $\vec{a}(\lambda_{\min})$ (or $\vec{a}(\lambda_{\max})$) onto the detector plane $D(\lambda)$. We define the region $A(\lambda)$ as a rectangular region bounded below by the straight line $v = v_{\min}(\lambda)$ and bounded above by the straight line $v = v_{\max}(\lambda)$. Let $\chi_{A(\lambda)}(u,v)$ denote the indicator function of $A(\lambda)$. In addition to the region B introduced to solve the SO problem, this region $A(\lambda)$ plays an important role in the proposed quasi-exact FBP algorithms for the LO problem. By using $A(\lambda)$, the first proposed algorithm is summarized as follows.

<Algorithm for LO Problem 1 (Algorithm LO-1)>

[STEP 1] Weighting (Eq. (2))

[STEP 2] Computation of Ramp Filtering Term (Eq. (3))

[STEP 3] Computation of Boundary Correction Term

$$g_2(u,v,\lambda) = \chi_{A(\lambda)}(u,v)g_1(u,v,\lambda) \tag{7}$$

$$S_\Delta^{(b)}(s,\mu,\lambda) = c_U(s,\mu)g_2^\mu(s,t_U,\lambda) + c_L(s,\mu)g_2^\mu(s,t_L,\lambda) \tag{8}$$

$$g^{Fb}(u,v,\lambda) = \frac{1}{4\pi^2}\frac{\partial}{\partial u}\int_{-\pi/2}^{\pi/2} d\mu S_\Delta^{(b)}(u\cos\mu + v\sin\mu,\mu,\lambda) \tag{9}$$

[STEP 4] Backprojection (Eq. (6))

The comparison between the Algorithm SO and the Algorithm LO-1 shows that we only need to multiply each cone-beam projection g_1 by the indicator function $\chi_{A(\lambda)}$ before computing the boundary correction term g^{Fb} in the LO problem. This can be done quickly in numerical implementation because $\chi_{A(\lambda)}$ does not depend on u and the explicit expression of $\chi_{A(\lambda)}$ is simple. Other parts (weighting, ramp filtering, and backprojection) do not need to be changed at all. Therefore, the Algorithm LO-1 can be easily implemented if one has a program for the Algorithm SO. Note that all the existing algorithms (L-ROI, ZB and VC) need rather complicated modifications in the structure of algorithms to deal with the long-object.

An alternative form of the Algorithm LO-1 can be obtained by performing the multiplication by $\chi_{A(\lambda)}$ before computing both the ramp filtering term and the boundary correction term. This leads to the following algorithm.

<Algorithm for LO Problem 2 (Algorithm LO-2)>

[STEP 1] Weighting

$$g_1(u,v,\lambda) = \frac{R}{\sqrt{R^2+u^2+v^2}}\chi_{A(\lambda)}(u,v)g(u,v,\lambda) \tag{10}$$

[STEP 2] Computation of Ramp Filtering Term (Eq. (3))

[STEP 3] Computation of Boundary Correction Term (Eqs. (4) and (5))

[STEP 4] Backprojection (Eq. (6))

Note that it is easy to verify that the Algorithm LO-1 and the Algorithm LO-2 produce a same reconstruction in the central ROI covered by the helix. This is thanks to the locality of ramp filtering. However, they produce different reconstructions in the region close to the end points of helix. The Algorithm LO-2 is also very simple. The comparison between the Algorithm SO and the Algorithm LO-2 shows that we only need to multiply each cone-beam projection g by $\chi_{A(\lambda)}$ before using the Algorithm SO to deal with the long-object.

C. Outline of Algorithm Derivation

Due to the lack of space, we only outline the derivation of the proposed algorithms. The algorithm derivation is

along the similar line to the derivation of the VC method [5]. It proceeds according to the following two steps. The first step is to construct the Radon algorithm by using the modified Grangeat formula (the Grangeat formula [7] which allows to combine triangular patches and half-planes to compute the 3-D Radon derivative). The second step is to reduce the Radon algorithm to the FBP form to verify that unmeasurable parts of projections used in the triangulation are unnecessary to reconstruct the central ROI when the helix is long enough to cover the ROI.

Let us consider the reconstruction of single point $\vec{r}_0$ in the central ROI. Let $\Pi(\vec{\xi}, l)$ denote a plane having the unit normal $\vec{\xi}$ and the radial distance l. Let $p'(\vec{\xi}, l)$ denote the 3-D Radon derivative over $\Pi(\vec{\xi}, l)$. From the inversion formula of 3-D Radon transform, we know that the reconstruction of $f(\vec{r}_0)$ needs $p'(\vec{\xi}, l)$ over a limited set of planes:

$$P = \{\Pi(\vec{\xi}, l) \mid l - \epsilon < \vec{r}_0 \cdot \vec{\xi} < l + \epsilon,\ \vec{\xi} \in \mathrm{S}^2,\ l \in \mathrm{R}\} \quad (11)$$

where ϵ is a small positive number [7]. By using this fact, the procedure for the algorithm derivation is outlined as follows.

[STEP 1] The triangulation for each $\Pi(\vec{\xi}, l) \in P$ is performed in the following way. Assume that the plane $\Pi(\vec{\xi}, l)$ intersects the helix at N points $\vec{a}(\lambda_1), \ldots, \vec{a}(\lambda_N)$. As shown in Fig. 1(a), we consider that the first source point $\vec{a}(\lambda_1)$ covers the lower half-plane which is below the line connecting $\vec{a}(\lambda_1)$ with $\vec{a}(\lambda_2)$, the last source point $\vec{a}(\lambda_N)$ covers the upper half-plane which is above the line connecting $\vec{a}(\lambda_{N-1})$ with $\vec{a}(\lambda_N)$, and other source points cover the triangular patches as in [2],[5].

[STEP 2] The mask function $\chi_{C(\lambda)}(u, v)$ on the detector plane $D(\lambda)$ to achieve the triangulation defined in [STEP 1] is derived. The resulting mask function depends on the source point $\vec{a}(\lambda)$. The forms of the mask function $\chi_{C(\lambda)}$ are illustrated in Fig. 1(b).

[STEP 3] We use the mathematical logic similar to [5] (reduction of the Radon algorithm to the FBP form) to show that unmeasurable parts of projections (which exceed the region B for the source points close to the end points of helix) are unnecessary to reconstruct the point $\vec{r}_0$. This clarifies that the filtered projections can be computed according to the following steps. Projections measured from the central part of helix are processed in the same way as in the Algorithm SO because $C(\lambda) = B$ for these projections. However, for projections measured from the source points close to the end point of helix $\vec{a}(\lambda_{\min})$ or $\vec{a}(\lambda_{\max})$, the boundary correction term must be included only from the subset $A(\lambda) \cap \partial B$. This is because $C(\lambda)$ for these projections is different from B and the corresponding boundary ∂B stops at some point $P_{\min}$ (or $P_{\max}$) defined by the cone-beam projection of the end point of helix $\vec{a}(\lambda_{\min})$ (or $\vec{a}(\lambda_{\max})$) onto the detector plane $D(\lambda)$ (Fig. 1(b)). Therefore, the boundary term from the missing boundary part must be excluded from the computation when processing these projections. This corresponds to truncate g_1 with the indicator function $\chi_{A(\lambda)}$ in the Algorithms LO-1 and LO-2. This is the rationale behind the use of new mask function $\chi_{A(\lambda)}$ in addition to χ_B in the LO problem.

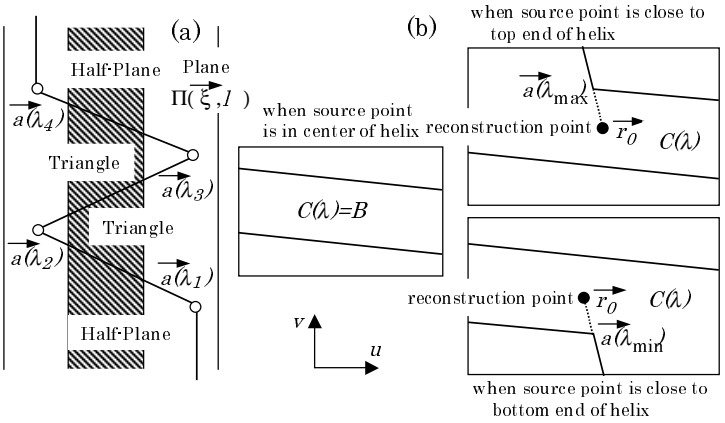

Fig 1: Illustration of triangulation for plane $\Pi(\vec{\xi}, l)$ and the corresponding mask function $\chi_{C(\lambda)}$.

III. Simulation Studies

We compared the proposed algorithms with the VC method [5] in terms of image quality, computational time, and simplicity of implementation. The same numerical phantoms as in [5] are used. The first phantom is the 3-D Shepp-Logan phantom to confirm how each algorithm reconstructs low-contrast objects. The second phantom is the disk phantom to confirm how each algorithm reconstructs high-contrast objects. These phantoms are supported inside the cylinder of radius 100 (mm). The number of helical turns is 2, the axial length of helix is 150 (mm) (pitch $2\pi h$ is 75 (mm)), and the radius of helix is 350 (mm). The number of cone-beam projections is 500 per turn and each projection consists of 256×93 detector pixels. Reconstructed images have 256×256×256 pixels. We have implemented the proposed algorithms as follows. As remarked in [2],[5], all the above algorithms are numerically unstable because they force to apply the ramp filtering across the boundary of region B. To overcome this numerical problem, we used the numerical stabilization technique based on smoothing the indicator function χ_B [2],[5]. This technique computes the filtered projection $g^{Fr} + g^{Fb}$ in the proposed algorithms as a sum of the three terms $g^F_{\text{ramp}} + g^F_{\text{fou}} + g^F_{\text{bound}}$ which can be computed in a stable way [2],[5]. Furthermore, we implemented both the single-ROI and multi-ROI algorithms proposed in [5].

Longitudinal slices of reconstructed images with the proposed algorithms (LO-1,LO-2) and the VC method are shown in Fig. 2. For the Algorithm LO-1, we also show reconstructed images with the multi-ROI implementation. The proposed algorithms could reconstruct high-quality images which are indistinguishable from those with the VC method. The main difference among the Algorithms

Fig 2: Reconstructed images with the VC single-ROI (first column), the LO-1 single-ROI (second column), the LO-2 single-ROI (third column), and the LO-1 multi-ROI (fourth column).

LO-1, LO-2, and VC seems to be the region on which accurate reconstruction can be achieved. Figure 2 shows that the LO-1 can obtain accurate images on a slightly larger region compared with the LO-2 and VC. This is thanks to the fact that the LO-1 discards less data compared with the LO-2 and VC because the multiplication by $\chi_{A(\lambda)}$ is applied only to the boundary correction term. Computational times are summarized in Table 1 (time for the approximate Feldkamp algorithm is also shown for comparison). The difference of reconstruction times among the LO-1, LO-2, and VC is not so much mainly because the dominant computation in all the algorithms is the 3-D backprojection which is common to all of them. In terms of simplicity, the proposed algorithms needed rather simple programming to implement compared with the VC method. In fact, a quite complicated routine to compute the boundary correction term in the VC method (Appendix C of [5]) could be completely eliminated. Thus, we believe that the proposed algorithms succeeded in dramatically reducing the complexity of implementation compared with the existing algorithms (L-ROI, ZB, and VC).

Table 1
Actual computational times measured by a SUN SPARC ULTRA-1 workstation with 256 M-byte memory.

Feldkamp (Full-Scan)	VC (Single)	LO-1 (Single)	LO-2 (Single)	LO-1 (Multi)
120(min)	412(min)	301(min)	296(min)	263(min)

IV. Conclusions

The proposed quasi-exact FBP algorithms for the LO problem are rather simple compared with the existing algorithms (L-ROI, ZB, and VC). The algorithms need only a few small changes to the quasi-exact FBP algorithm for the SO problem derived by Kudo *et al* [2]. We will present additional simulation results with more challenging Schaller's head phantom at the conference.

V. References

[1] K.C.Tam, S.Samarasekera, and F.Sauer "Exact cone-beam CT with a spiral scan," *Phys.Med.Biol.*, Vol.43, pp.1015-1024, 1998

[2] H.Kudo, F.Noo, and M.Defrise "Cone-beam filtered backprojection algorithm for truncated helical data," *Phys.Med.Biol.*, Vol.43, pp.2885-2909, 1998

[3] S.Schaller, F.Noo, F.Sauer, K.C.Tam, G.Lauritsch, and T.Flohr "Exact radon rebinning algorithms using local region-of-interest for helical cone-beam CT," *IEEE Trans.Med.Imaging*, Vol.19, pp.361-375, 2000

[4] M.Defrise, F.Noo, and H.Kudo "A solution to the long-object problem in helical cone-beam tomography," *Phys.Med.Biol.*, Vol.45, pp.623-643, 2000

[5] H.Kudo, F.Noo, and M.Defrise "Quasi-exact filtered backprojection algorithm for long-object problem in helical cone-beam tomography," *IEEE Trans.Med.Imaging*, Vol.19, pp.902-921, 2000

[6] K.C.Tam "Exact local regions-of-interest reconstruction in spiral cone-beam filtered-backprojection CT: theory," *Proc. SPIE Medical Imaging*, Vol.3979, pp.506-519, 2000

[7] P.Grangeat "Mathematical framework of cone-beam 3D reconstruction via the first derivative of the Radon transform," in Mathematical Methods in Tomography, G.T.Herman, A.K.Louis, and F.Natterer Eds., Springer, 1991, pp.66-97